Contents lists available at ScienceDirect

Food Packaging and Shelf Life

journal homepage: http://ees.elsevier.com

Water vapor barrier properties of wheat gluten/silica hybrid coatings on paperboard for food packaging applications

Cesare Rovera [a], Hasan Türe [b], Mikael S. Hedenqvist [c], Stefano Farris [a,*]

[a] DeFENS, Department of Food, Environmental and Nutritional Sciences, University of Milan, via Celoria 2 – I-20133, Milan, Italy
[b] Fatsa Faculty of Marine Science, Department of Marine Science and Technology Engineering, Ordu University, Ordu, Turkey
[c] Department of Fibre and Polymer Technology, School of Engineering Sciences in Chemistry, Biotechnology and Health, KTH Royal Institute of Technology, Stockholm, 10044, Sweden

ARTICLE INFO

Keywords
Brittleness
Moisture sensitivity
Sol-gel
Thermal properties
Wettability
Wire wound rod

ABSTRACT

Motivated by the increasing need for new solutions with less environmental impact, in this work we have investigated the benefits of depositing a wheat gluten (WG) coating on paperboard substrates intended for food packaging applications. To overcome the inherent moisture sensitivity of this protein, WG was combined with a silica network obtained by sol-gel chemistry. WG/silica hybrid coatings were characterized in terms of structural, thermal, morphological, surface, and water vapor barrier properties. Spectrometric analysis demonstrated that the organic and inorganic phases interacted primarily through hydrogen bonding. This was also supported by thermal experiments, which revealed a higher T_g measured for the hybrid materials with the higher silica content (114 ± 1 °C and 128 ± 2 °C, respectively) compared to the pure WG material (T_g = 89 ± 1 °C). Scanning electron microscopy showed that the surfaces of the coatings were very smooth, though the presence of pinholes, cracks, fractures, and voids was detected, especially for the silica-rich formulations. Upon deposition of the coatings, the wettability of the bare paperboard increased, as demonstrated by the lower water contact angle values. In addition, hybrid coatings exhibited a higher wettability over the pristine WG coating, which was due to a more intense spreading phenomenon. The deposition of the coatings led to a ~ 4-fold reduction in water vapor transmission rate (WVTR ~ 90 g m^{-2} 24 h^{-1} at 23 °C and 65% relative humidity) of the specific cellulosic substrate tested in this work (WVTR ~ 350 g m^{-2} 24^{-1}).

1. Introduction

The increased attention to environmental concerns has recently prompted a renewed interest in cellulosic materials, including paper and paperboard, which have been used in numerous applications for centuries. Over time, the use of cellulosic materials has spread, and today, these materials are used by a wide range of industries. In the packaging industry, one of the most economically important applications of cellulosic materials is in the food sector. Paper and paperboard encompass 31% of the global packaging market and are mainly used in food packaging for containment and protection of the food products, convenience during storage or consumption, and communication of the relevant information to consumers, including marketing aspects (Jones & Comfort, 2017). Widespread uses of paper and paperboard concern ice-cream cups, microwave popcorn bags, baking paper, fast food containers such as pizza, beverage cups etc. (Deshwal, Panjagari, & Alam, 2019). In these cases, the main goal of the packaging material is to act as a container, enabling some specific actions such as cooking, handling, and easy consumption of the food. In other applications as primary packaging (i.e., in direct contact with food), paper is a component of a packaging configuration specifically designed to protect the food and extend its shelf life. This is the case, for example, of dry biscuits, milk cartons, chips, juices, fruit, vegetables, bread etc. However, in all the above applications the paper layer is coupled with other layers (most often plastic layers) mainly because paper alone is very high sensitivity to gases (e.g. oxygen and carbon dioxide) and vapors (e.g. water vapor and aromas), which diffuse through the highly porous material (Krook & Hedenqvist, 2002).

Many efforts have been made to address this issue over the years, especially via physical and chemical methods, in an attempt of increasing the utility of cellulosic materials for a wider range of applications. For example, cellulosic substrates have been coupled to various non-cellulosic materials, such as: plastic polymers (e.g. polyethylene – PE and polyethylene terephthalate – PET); natural waxes; and aluminum foil (Deshwal et al., 2019; Mir, Wani, Wani, Singh, & Wani, 2017). Today, these coupling procedures are usually performed by co-extrusion or lamination to obtain multi-layer cellulosic-based materials with barrier properties against water vapor, grease, and oxygen, mak-

* Corresponding author.
E-mail address: stefano.farris@unimi.it (S. Farris)

https://doi.org/10.1016/j.fpsl.2020.100561
Received 29 February 2020; Received in revised form 18 July 2020; Accepted 25 August 2020
Available online xxx
2214-2894/

ing them suitable for most packaging applications (Das et al., 2018). However, lamination of paperboard with plastics or aluminum foil decreases the recyclability of the final product.

The ability to improve the overall properties of cellulosic substrates through biopolymer materials is becoming increasingly important for both the scientific and industrial communities, enabling these materials to serve as attractive alternatives to polymers of fossil origin. In particular, improving the barrier properties of cellulosic materials, without jeopardizing their inherent degradability, remains a major challenge. To this end, several solutions have been tested, such as polycaprolactone – PCL (Bota, Kratofil, Katančić, Brozović, & Hrnjak-Murgić, 2017), polylactic acid – PLA (Rhim, Lee, & Hong, 2007), and many natural hydrocolloids in the form of aqueous dispersion coatings including starch, cellulose derivatives, chitosan, alginate, whey proteins, caseinates, zein, soy protein, and wheat gluten (Andersson, 2009; Gällstedt, Brottman, & Hedenqvist, 2005; Gatto, Ochi, Pedroso Yoshida, & Ferreira da Silva, 2019; Mazhari Mousavi, Afra, Tajvidi, Bousfiled, & Dehghani-Firouzabadi, 2017; Menzel & Koch, 2014; Mirmehdi, Gherardi Hein, Grígoli de Luca Sarantópoulos, Dias, & Denzin Tonoli, 2018; Ottesen et al., 2017; Zhang, Xiao, & Qian, 2014).

Among biopolymers, the interest towards wheat gluten (WG) lies in its functional properties, wide availability and low cost since it is a by-product of starch production for e.g. ethanol biofuel (Farrell et al., 2006; Lens et al., 2003). In addition, WG displays suitable material properties as well as good biodegradability (Sartori, Feltre, do Amaral Sobral, Lopes da Cunha, & Mengalli, 2018). Besides the above-mentioned advantages, the long-lasting interest in WG for food packaging applications is mainly due to its good barrier properties against gases (e.g., oxygen and carbon dioxide) in dry conditions, which make WG a viable solution to control the inherent permeability to gas of cellulosic materials (Gontard, Guilbert, & Cuq, 1992; Guillaume, Pinte, Gontard, & Gastaldi, 2010; Gontard, Thibault, Cuq, & Guilbert, 1996; Hedenqvist, 2018; Mujica Paz & Gontard, 1997; Mujica Paz, Guillard, Reynes, & Gontard, 2005; Olabarrieta et al., 2006). However, a drawback is the high sensitivity to moisture, which causes a marked decrease of the gas barrier properties at high relative humidity, restricting its potential use to breathable foods, such as fruit and vegetables. This is why, for example, gluten films/coatings tend to swell when in contact with aqueous media. For the same reason, the water vapor permeability values for WG films were reported to be 2-5 orders of magnitude greater than those of typical polymeric packaging films, such as polypropylene (PP), polyethylene (PE), polyvinylidene chloride (PVC), and polyethylene terephthalate (PET) (Gennadios, Brandenburg, Park, Weller, & Testin, 1994). As widely reported in the literature, this is primarily due to the inherent hydrophilic nature of the WG protein as well as to the substantial amount of hydrophilic plasticizer (e.g. glycerol) generally added to impart adequate film flexibility (Tunc et al., 2007).

To date, many different approaches have been used to address the water sensitivity of WG materials, including coating a thin layer of polyethylene terephthalate, thermal treatment-mediated polymer network modifications, the use of mixed WG and hydrophobic biodegradable polymers (e.g. polycaprolactone), mixing WG with polysaccharides to yield structural complexes, or incorporation of nanofillers such as montmorillonite (Das et al., 2020; Mascheroni, Guillard, Gastaldi, Gontard, & Chalier, 2011; Sartori et al., 2018; Türe, Gällstedt, Johansson, & Hedenqvist, 2013). In the present study, we propose an alternative approach to improve the water vapor barrier properties of paperboard, based on the development of WG-based hybrid coatings through sol-gel chemistry. This approach is widely adopted in the coating technology because of its versatility, low cost, and low environmental impact, especially compared to hard-chemistry synthesis routes (Rovera, Ghaani, & Farris, 2020). For example, hybrid coatings were obtained by sol-gel chemistry to improve the oxygen barrier properties of plastic films (Farris et al., 2012; Fuentes-Alventosa et al., 2013; Startek, Marczak, & Lukowiak, 2020). Sol-gel hybrid coatings were also prepared to obtain antimicrobial (Corradini et al., 2013; Lantano et al., 2014; Razavi, Tajik, Moradi, Molaei, & Ezati, 2020), antioxidant (Bossi, Tana, Punta, Cigada, & De Nardo, 2016) and intelligent (Liu et al., 2020) food packaging materials. In these previous works, the inorganic phase (silica-based) was used in combination with an organic counterpart represented by a biopolymer, such as pullulan, chitosan, poly-lysine, etc. However, to our knowledge, the use of the sol-gel technology to improve the water vapor barrier performance of WG coatings on cellulosic substrates intended for food packaging applications has never been reported before.

2. Fundamental chemistry underlying development of WG-silica hybrid materials

The use of the sol-gel approach is widely used in the coating technology to obtain hybrid materials with high performance, in spite of the reduced thickness of the final layer (from tenths of nm up to few microns) (Rovera et al., 2020). More recently, the sol-gel technology has been extended for the generation of hybrid coatings obtained from metal alkoxides (e.g., tetraethoxysilane, TEOS) in combination with biopolymers (Razavi et al., 2020). The overall process accounts for two main steps, i.e. hydrolysis and condensation (Fig. 1). Hydrolysis occurs by the nucleophilic attack of the oxygen contained in water on the silicon atom, according to the reaction scheme reported in Fig. 1a. However, protonation of alkoxide groups is faster if an acid is used as a catalyst, although the base-catalyzed hydrolysis is also well established (Schubert, 2015). Alkoxide groups (–OR) of the precursor are then replaced with hydroxyl groups (-OH) to form the silanol compounds -$Si(OH)_n$, whereas ethanol is the by-product.

Upon hydrolysis and in presence of the organic phase, two main different pathways can possibly involve the silanol groups. On one hand, $Si(OH)_n$ may react according to a typical condensation scheme by two different routes (water condensation and alcohol condensation) to yield in both cases SiO_2 covalent bonds and water or alcohol as by-products (Fig. 1b). On the other hand, the $Si(OH)_n$ groups can interact by secondary forces (e.g., hydrogen bonds) with the pendant polar group along the backbone of the organic polymer (Farris et al., 2012). In this work, we assumed that hydrogen bonding can occur between the polar groups of most abundant wheat gluten amino acids (e.g. –OH and $–NH_2$ groups of glutamic acid, aspartic acid, serine, threonine, asparagine, arginine, lysine) and the silanol groups, which will simultaneously form the glass-like oxidic network by new SiO_2 covalent bonds (Fig. 1c). Eventually, both the *in-situ* synthesis of SiO_2 in the WG water dispersions and the hydrogen bonds formation can explain the overall performance that is expected in the final hybrid materials.

3. Materials and Methods

3.1. Reagents and chemicals

Commercial wheat gluten powder was kindly supplied by Lantmännen Repper AB, Sweden. According to the supplier, the gluten protein content was 77.7 wt% (dry basis) (modified NMKL Nr 6, Kjeltec, Nx5.7, www.NMKL.org), the moisture content was 6.9 wt% of the total weight (NMKL 23, 1991), and the starch content was 5.8 wt% (dry basis) (Ewers, polarimetric method). The concentration of fats was 1.2 wt% (dry basis) (Soxtec, Lidfett.OA.19, tecator AN 301), and the ash content was 0.9 wt% (dry basis) (NMKL 173 2nd ed). High purity TEOS (Sigma-Aldrich, Stockholm, Sweden) was used as a metal alkoxide precursor of the inorganic phase; 1 M hydrochloric acid (Sigma-Aldrich, Stockholm, Sweden) was used as a catalyst. Pure acetic acid and sodium sulphite (Sigma-Aldrich, Stockholm, Sweden) were used to prepare the wheat gluten dispersions. Paperboard samples (Korsnäs Du-

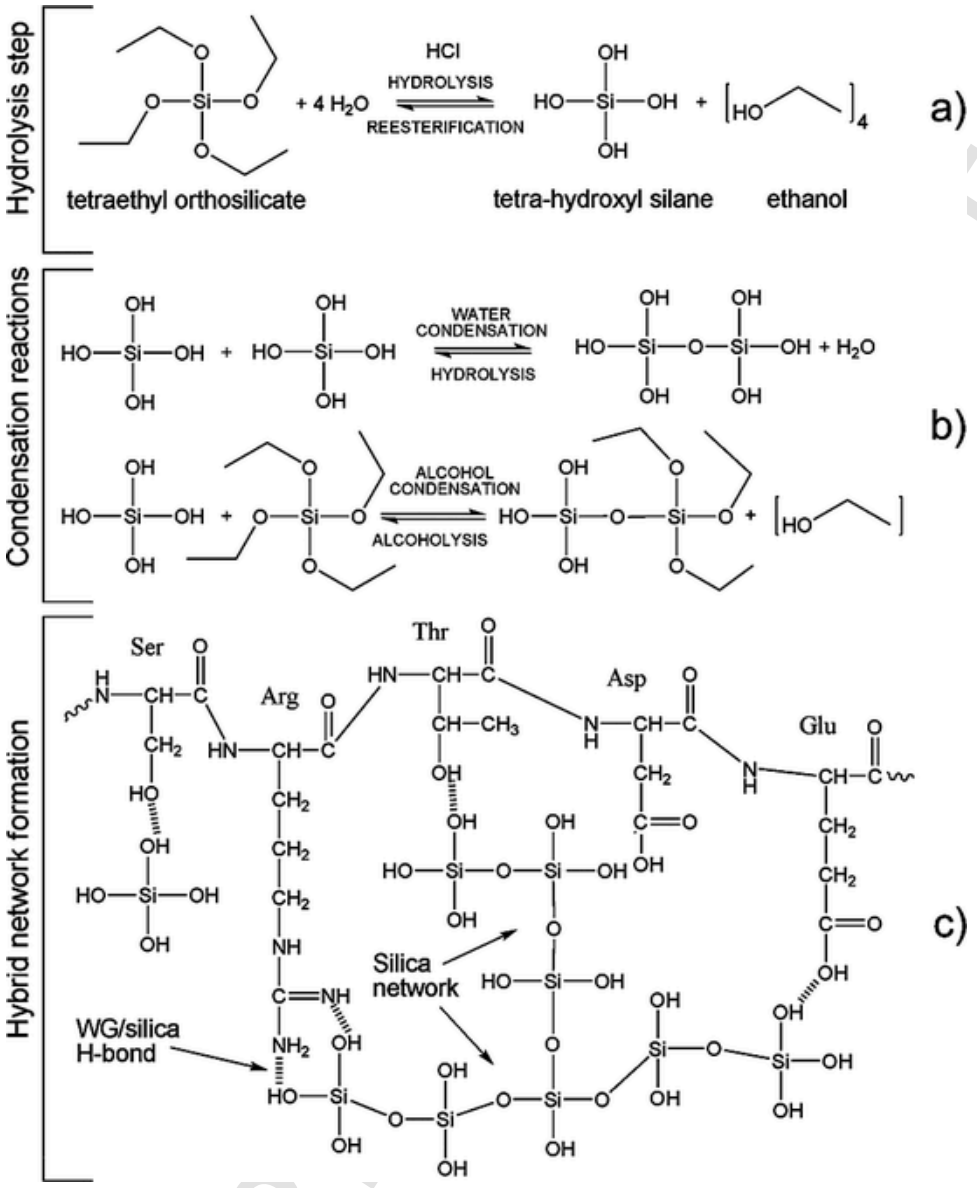

Fig. 1. Schematic representation of the hydrolysis (a) and condensation (b) reactions; and the hybrid network formation between an exemplificative 5-amino acids sequence (Ser-Arg-Thr-Asp-Glu) of the WG protein and the silica network.

plex 260) were provided by Korsnäs AB, Gävle, Sweden. The bottom layer of the paperboard, which was used as a substrate for the coatings, consisted of unbleached softwood sulphite pulp, while the middle layer consisted of unbleached chemithermomechanical pulp (CTMP). The top hydrophobic layer consisted of a blend of bleached softwood and hardwood, which was treated using a dual glue, containing alkyl ketene dimer (AKD) and resin glue. The thickness of the paperboard samples ranged between 350 μm and 400 μm. Ethanol (Sigma-Aldrich, Milan, Italy) and Milli-Q water (18.3 MΩ · cm) were used for the hybrid coating dispersion preparations. All materials were used as received.

3.2. Preparation of hybrid coatings

Hybrid coatings were prepared according with the procedure proposed by Türe et al., with slight modifications (Türe, Blomfeldt, Gällstedt, Hedenqvist, & Farris, 2013). Briefly, an acidic (pH = 2.0 ± 0.8) hydro-alcoholic (30 wt% ethanol) solution of TEOS was prepared using 1 M HCl (0.78 wt%) as a catalyst, with a fixed H_2O:TEOS molar ratio of 4:1. TEOS hydrolysis was conducted at room temperature for approximately 1 hour. At the same time, an aqueous dispersion of wheat gluten was prepared at room temperature, by mixing gluten powder into water containing sodium sulphite (2.5 mg/g wheat gluten) as a reducing agent, for 30 minutes under gentle stirring (500 rpm). Acetic acid was then added to the mixture in order to adjust the pH to 4.0. Air bubbles possibly formed during stirring were removed using a sonicator bath (mod. 2510, Branson, Danbury, USA) at room temperature for 2 minutes. The inorganic and organic phases were then mixed together for 1 hour, to facilitate formation of the hybrid network. To investigate the influence of the organic/inorganic ratio (O/I, defined as the wheat gluten/$(SiOH)_4$ weight ratio for a complete hydrolysis process) on the final water vapor barrier properties of the composites, six different coating dispersions were prepared, by varying the O/I ratio of the coatings from 100/0 to 50/100, as reported in Table 1. Note that subscripts indicate the O/I ratio (for example, H_1 stands for hybrid with O/I = 1). The composite solutions were then deposited onto the paperboard samples using a steel horizontal wire wound rod (S26, RD Specialties Inc, Webster, NY), with a wire diameter of 660 μm, enabling deposition of a wet thickness of 59 μm (i.e.

Table 1
Formulation parameters of the WG-based coatings used in this work.

Exp. n°	Code Name	WG (wt-%)	$Si(OH)_4$ (wt-%)	(O/I*) ratio
1	Neat paperboard	0	0	/
2	H_0	20	0	/
3	H_3	15	5	3
4	H_2	13.3	6.7	2
5	H_1	10	10	1
6	$H_{0.75}$	8.6	11.4	0.75
7	$H_{0.5}$	6.7	13.3	0.5

* "I" refers to the silanol form – $Si(OH)_4$, calculated from the initial TEOS content and assuming completion of the hydrolysis reaction. Roman superscripts denote statistically significant differences ($p < 0.05$).

a dry thickness of approximately 12 μm for a water-based 20 wt% dispersion, assuming a density equal 1 g cm^{-3}). Coated paperboard samples were dried first by using a constant and perpendicular flux of mild air (25.0 °C ± 0.3 °C) at a distance of 40 cm from the applicator for 2 min. In the second step, composite films were stored in an oven at 40 °C for 24 hours.

3.3. Fourier Transform Infrared – Attenuated Total Reflectance (FTIR-ATR) Analysis

Physicochemical properties of WG coatings at different silica concentrations were investigated using a PerkinElmer FT-IR Spectrum™ 100 Series spectrometer (PerkinElmer, Waltham, MA, USA) equipped with a universal attenuated total reflectance (UATR) accessory with the single-reflection sampling plate of 1.8 mm round germanium surface. To ensure satisfactory physical contact between samples and crystal surface, a high-pressure clamping device was used. Spectra were recorded at room temperature within the range of 600–4000 cm^{-1} at 4 cm^{-1} resolution. Spectrum 6.0 software was used for data acquisition and analysis.

3.4. Thermal properties

The thermal properties of both WG and hybrid film samples were determined by differential scanning calorimetry (DSC) analysis using a DSC 1 (Mettler Toledo, Columbus, OH) supplied with a quench-cooling accessory and a GC 100 gas controller. Before measurements, the instrument was calibrated with the well-characterized standard indium, which has a heat of fusion (ΔH) of 28.4 J/g and a melting temperature (T_m) of 156.6 °C. Approximately 5 mg of WG or WG/silica samples were then put in aluminum pans (40 μL) which was hermetically sealed and holed to allow the entrance of the purge gas. All the thermograms were obtained in an inert environment (50 mL min^{-1} N_2) at a rate of 10 °C min^{-1}. An initial scan from -50 to 300 °C was followed by an isothermal step (300 °C for 5 min), with the goal of removing the residual moisture. Samples were then cooled down to −50 °C to erase the thermal history. A second heating scan was finally carried out from -50 to 300 °C for the determination of the glass transition temperature (T_g). For the determination of the specific heat capacity (c_p) of pure WG and hybrid materials, the same protocol as above was used, with the exception of the final temperature of the heating cycle, which was set at 180 °C to avoid any possible influence on the c_p due to thermal degradation of the matrix.

3.5. Field-Emission Scanning Electron Microscopy (FE-SEM)

Both the coated surfaces and cross-sections of the films were examined using a Hitachi S-4800 FE-SEM. Samples were dried in a desiccator in the presence of silica gel for a minimum of 48 h before examination. Surface test specimens were mounted with carbon tape on stubs. Cross-sectioned samples were cut into thin pieces with a scalpel, and mounted on a Hitachi thin specimen split mount holder, M4 (prod. No 15335-4), to observe the cross-section and determine the thickness of the coating. Before insertion in the microscope, samples were coated with gold to a thickness of ca. 10 nm (to avoid charging the samples), using an Agar High Resolution Sputter Coater (model 208RH), equipped with a gold target/Agar thickness monitor controller.

3.6. Optical Contact Angle (OCA)

The wettability of the coated surfaces was assessed using an optical contact angle apparatus (KSV CAM 200, Espoo, Finland), equipped with a Basler A602f camera. The contact angle of water in air was measured on rectangular (5 × 2 cm^2) coated paperboard samples by the sessile drop method. This method consists of gently dropping a droplet of 4 ± 0.5 μL of Milli-Q water (18.3 MΩ cm) onto the coated surface, according to the so-called pick-up procedure. Specifically, a droplet hanging on the end of a needle is laid on the coating surface by raising the sample stage until solid/liquid contact is made. Analyses were conducted in a climate-controlled room (23 °C and 50 % relative humidity (RH)). All droplets were released from a height of 1 cm above the surface, to ensure consistency between each measurement. The evolution of the contact angle (θ, the angle between the baseline of the drop and the tangent at the drop boundary), the droplet volume (V, μL) and the droplet surface area (A, mm^2), were monitored using a software-assisted image processing procedure, which fits the drop profile with the Young-Laplace equation. The values of these parameters were collected 2 times per second during the first 10 seconds and 1 time per second during the following 50 seconds of analysis, starting from the deposition of the drop (t_0 = 0 s) to 60 s (t_{60} = 60 s). A minimum of 10 droplets were examined for each sample on both the left and right sides, and resulting mean θ values were then used for the calculations described below.

3.7. Water vapor barrier properties

Water vapor transmission rates (WVTR) of both uncoated and coated paperboard samples were assessed using a Multiperm permeability analyzer (ExtraSolution® Srl, Capannori, Italy) equipped with an infrared sensor and based on the isostatic method. Specimens were sandwiched between two aluminum-tape masks, allowing a surface of 2.01 cm^2 to be exposed to the permeation of water vapor. WVTR values (g m^{-2} 24 h^{-1}) were determined using the standard method ASTM F1249, with a carrier flow (N_2) of 10 mL min^{-1}. Measurements were performed at 23 °C and 65 % RH, which is the humidity gradient between the two semi-chambers between which the sample was mounted. Each WVTR value was from five replicates.

3.8. Statistical analysis

Data were analyzed using Statgraphics Plus 4.0 software (STSC, Rockville, MD, USA), and one-way analysis of variance was used to check for differences between samples. The significance level (p) was fixed at 0.05.

4. Results and Discussion

4.1. Thickness of the composites

SEM micrographs (Fig. 2) revealed that all samples were slightly thinner than theoretically predicted, with an average value of 9.5 ± 1.5 μm, rather than ~ 12 μm (assuming a 20 wt% dry matter content in the dispersion). The variability was quite high (relative stan-

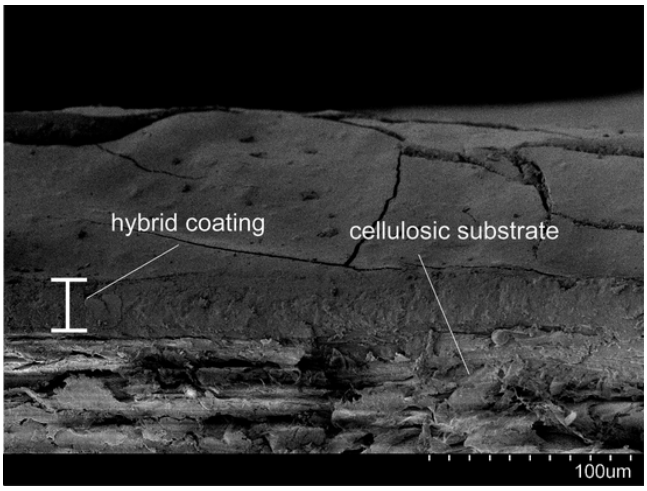

Fig. 2. Representative cross-section scanning electron microscopy image (400×) of a paperboard-hybrid coating composite produced in this work.

dard deviation ~ 30%) within samples (i.e., for a same sample), which may be due to the highly heterogeneous surface of the paperboard and to an uneven distribution of the coating throughout the fibrous surface. In addition, the difference between theoretical and measured thickness values appears to be more pronounced with increasing O/I ratio, which was probably due to the increasing amount of ethanol as a by-product of the condensation step of the sol-gel reaction. However, no statistically significant difference was observed between samples. We also determined the grammage of the coating (coating weight per unit surface, g/m^2) gravimetrically, i.e., weighing 1 dm^2 of the cellulosic substrate with and without coating, the difference being then scaled to 1 m^2, according to Gatto et al. (2019). The average grammage of the coatings was 10.5 ± 1.5 g/m^2, with no statistically significant difference among formulations. The final appearance of all composites (i.e. paperboard + coating) indicated a bi-layer structure, with no clear evidence of interpenetration between the two contacting layers.

4.2. WG–silica hybrids formation

FT-IR can provide detailed information on the nature of interphase bonding. FT-IR spectra of pure wheat gluten and reacted TEOS (i.e., after hydrolysis and condensation) have been discussed elsewhere (Türe, Blomfeldt et al., 2013; Türe, Gällstedt et al., 2013). Fig. 3a–c show the three spectral regions that underwent the most significant changes as a function of O/I ratio. Association of the two phases produced dramatic changes in the FT-IR spectra of the resulting hybrid coatings. For clarity, each of the three spectral regions which underwent significant changes is discussed separately below.

In the region (3850 cm^{-1} – 2400 cm^{-1}, Fig. 3a) decreasing the O/I ratio (i.e., moving from the formulation H_3 to $H_{0.5}$) resulted in a broadening of the band at ~ 3300 cm^{-1} assigned to amide A and B (N-H stretching vibration) of WG. This mode of vibration has been shown to be independent of backbone conformation, but is very sensitive to hydrogen bond strength (Krimm & Bandekar, 1986). Accordingly, peak broadening in this region could possibly be due to extensive hydrogen bonding between silanol and hydroxyl groups of the organic phase (Bandyopadhyay, De Sarkar, & Bhowmick, 2005; Lee, Lee, & Yang, 1999; Tong, Xiao, & Lim, 2008).

The second region (1720 – 1470 cm^{-1}, Fig. 3b) contains the two major bands of the protein infrared spectrum: amide I (~ 1650 cm^{-1}) and amide II (~ 1530 cm^{-1}), whose peak intensities are directly influenced by the backbone conformation (the secondary structure of the protein). As can be seen in the inset in Fig. 3b, even the lowest concentration of silica tested (O/I = 3) produced significant changes

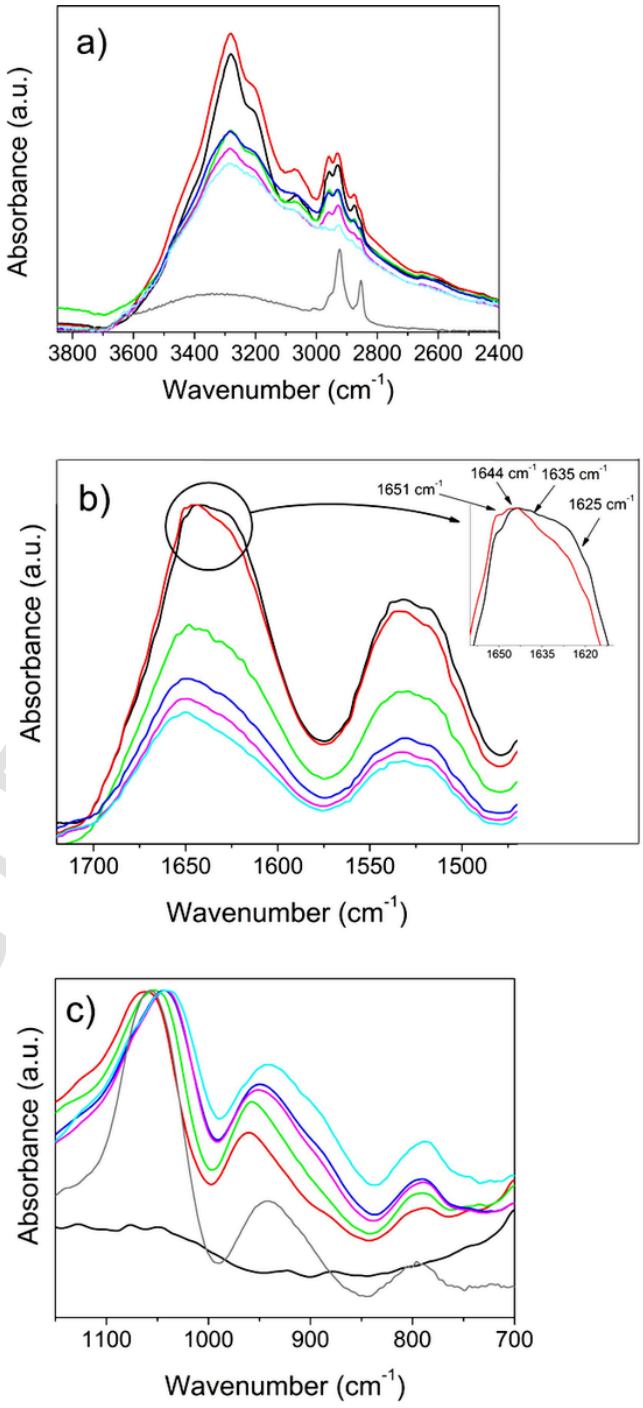

Fig. 3. FTIR-ATR spectra of hybrid coatings within 3850 cm^{-1} ÷ 2400 cm^{-1} (a), 1720 ÷ 1470 cm^{-1} (b), and 1150 cm^{-1} ÷ 700 cm^{-1} (c) spectral ranges. Symbols: ( ) pure WG; ( ) reacted TEOS; ( ) H_3; ( ) H_2; ( ) H_1; ( ) $H_{0.75}$; ( ) $H_{0.5}$.

in the amide I band, which is intimately related to the physical structure of the wheat gluten chains. More specifically, the bands at 1651 cm^{-1} and 1644 cm^{-1} can be assigned to α-helices/random coils and disordered domains, respectively; while bands at 1635 cm^{-1} and 1625 cm^{-1} are attributed to β-sheet conformations with a high or low level of hydrogen bonding, respectively (Cho, Gällstedt, & Hedenqvist, 2010; Cho, Gällstedt, Johansson, & Hedenqvist, 2011). The addition of the inorganic phase reduced the width of the peak assigned to amide I from 1640 cm^{-1} to 1620 cm^{-1} (see the inset in Fig. 3b). Simultaneously, the peak centered at 1651 cm^{-1} increased considerably in the H_3 sam-

ple, and even more markedly in the other hybrid coatings, with decreasing O/I ratio. These observations clearly demonstrate that the presence of the inorganic phase has a 'destructuring' effect on the main WG network. More specifically, the presence of silica interferes with the formation of an ordered secondary structure, increasing the proportion of random coil and disordered regions in the WG matrix, confirming our previous findings obtained on WG/silica 3D hybrid materials (Türe, Blomfeldt et al., 2013; Türe, Gällstedt et al., 2013).

In the third region (1150 cm^{-1} – 700 cm^{-1}, Fig. 3c), the band centered at ~945 cm^{-1}, which was assigned to silanol groups (Si–OH) in the reacted TEOS spectrum, shifted toward higher wavenumbers, especially in the case of the H_3 formulation (peak centered at 962 cm^{-1}). In addition, the extent of this shift is gradually reduced as the O/I ratio is decreased; and for sample $H_{0.5}$ no shift was observed. These results are in contrast to those previously reported for pullulan/silica hybrid coatings, where shifting of the same peak toward higher wavenumbers with increasing inorganic phase was attributed to a corresponding increase in hydrogen bonding between the organic and inorganic phases (Farris et al., 2012). Interestingly, the peak assigned to silicon oxide (SiO_2) asymmetric stretching (~1060 cm^{-1}) shifted to a slightly higher wavenumber (1064 cm^{-1}) at the lowest silica concentration; while a shift toward lower wavenumbers was observed as the O/I ratio decreased, up to 1040 cm^{-1} for the sample $H_{0.5}$. Therefore, it is likely that other forces in addition to hydrogen bonding are responsible for driving the interactions between the two phases (organic and inorganic); because, although O/I < 3 was mostly driven by hydrogen bonding, decreasing the O/I ratio promoted different interactions involving the SiO_2 network. This hypothesis seems to be supported by the disappearance of peaks centered at 1730 cm^{-1} and 1233 cm^{-1}in the pure WG spectrum, which might reflect either the establishment of new bonds involving carbonyl groups along the WG backbone, or interaction of the silica with WG reactive groups (e.g. –OH groups) to form Si-O-C bonds, as already postulated for polyvinyl alcohol/silica hybrids (Minelli, De Angelis, Doghieri, Rocchetti, & Montenero, 2010; Uragami, Okazaki, Matsugi, & Miyata, 2002). However, whether these new bonds in the hybrid coatings can be considered to be covalent in nature is still under investigation.

4.3. Differential Scanning Calorimetry

DSC analyses were performed with the goal of corroborating the information obtained from the FT-IR test concerning the structural changes in the WG network upon interaction with the inorganic phase. Fig. 4 displays the DSC traces of pure WG samples and of the hybrid materials containing an equal amount (H_1) and twice the amount of ($H_{0.5}$) of silica compared to that of WG. In the first heating scan (Fig. 4a) a main endothermal region above 200 °C can be observed for the three samples, with a sharp peak centered at 216 ± 1 °C, 239 ± 2 °C, and 271 ± 2 °C for the samples H_0, H_1 and $H_{0.5}$, respectively. The shift of the endothermal peak to higher temperatures moving from the formulation H_0 to the formulation $H_{0.5}$ is a clear evidence of the protective role of silica in terms of thermal stability of the WG network, confirming what was observed for WG-silica biofoams (Wu et al., 2014). Samples H_0 and H_1 also showed a second endothermal peak (at 264 ± 1 °C and 256 ± 2 °C, respectively) (Fig. 4a), which was not detected in sample $H_{0.5}$, probably because of the protective role of silica. These endothermic peaks at relatively high temperatures can be attributed to the thermal degradation of the main polymer phase, with special reference to the functionalities of the protein primary structure. This is in agreement with previous TGA experiments, which showed the degradation of the pure WG sample occurred in two main temperature regions, whereas in the hybrid composites most weight loss occurred

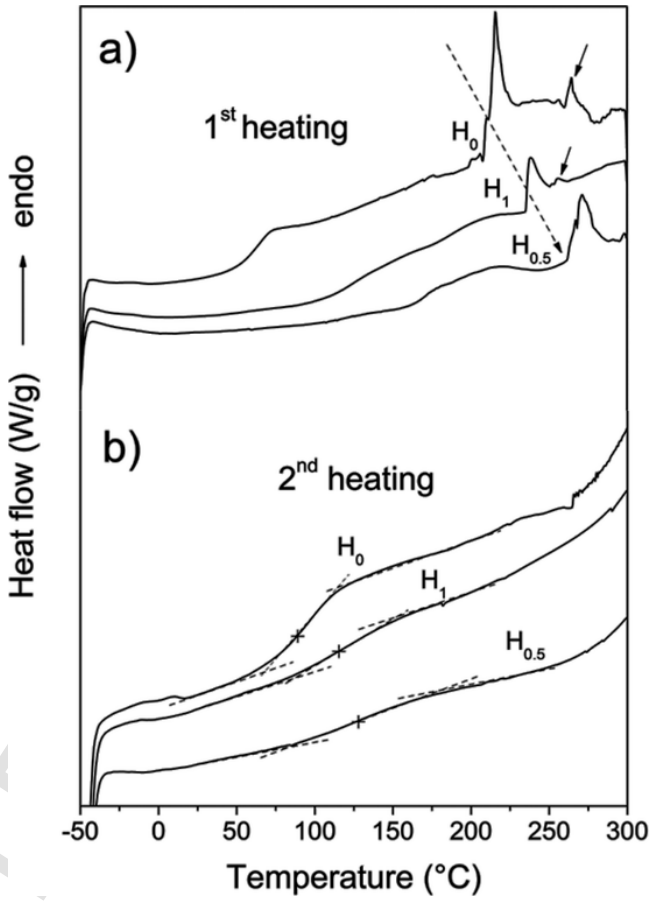

Fig. 4. First heating (a) and second heating (b) DSC traces of the pure WG (H_0) and the hybrid (H_1 and $H_{0.5}$) materials.

in only one step (Türe, Blomfeldt et al., 2013; Türe, Gällstedt et al., 2013).

The second heating scan (Fig. 4b) revealed differences in the second order transition experienced by the samples. The higher T_g measured for the hybrid materials H_1 and $H_{0.5}$ (114 ± 1 °C and 128 ± 2 °C, respectively) compared to the pure WG material H_0 (T_g = 89 ± 1 °C) can be explained as a consequence of the new interactions (hydrogen bonds) between the two phases, hence confirming what the findings arising from the FT-IR analyses. These new bonds would have eventually restricted the segmental mobility of the molecular chains within the amorphous regions, thus increasing the glass transition temperature.

A quantitative determination of the specific heat capacity (c_p) of the different materials was possible considering the inflexion in the base line of DSC thermograms obtained from -50 °C to 180 °C, and using the general equation for the total heat flow at any point in a DSC experiment given by (Hatakeyama & Quinn, 1999):

$$\frac{\partial Q}{\partial t} = C\,\beta + f(T,t) \quad (1)$$

where: $\partial Q/\partial t$ (J min^{-1}) is the heat flow, that is, the amount of heat transferred per unit time; C (J K^{-1}) is the sample heat capacity; β (K min^{-1}) is the constant heating rate; $f(T, t)$ is the heat flow associated to the kinetic processes that are (absolute) temperature and time dependent. The heat capacity component of the total heat flow, $C\,\beta$, is generally referred to as the reversing heat flow, while the kinetic component, $f(T, t)$, being referred to as the non-reversing heat flow. Therefore, the specific heat capacity (c_p) profile in the second order transition region (i.e. where the kinetic component can be assumed to be equal to

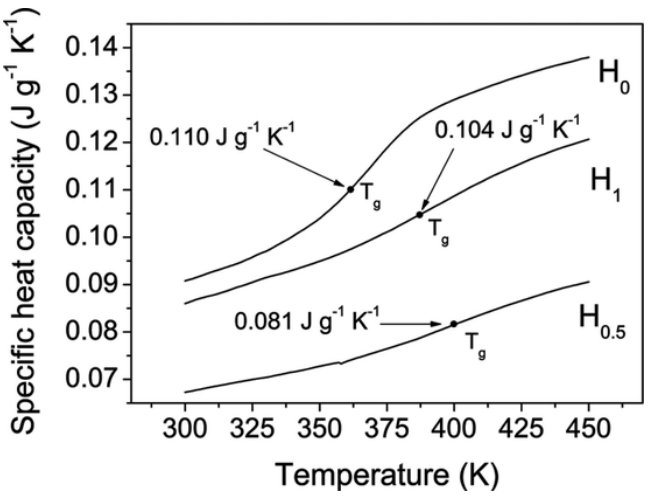

Fig. 5. Specific heat capacity (c_p) profile of pure WG and hybrid materials H_1 and $H_{0.5}$ within the temperature range 300 K – 450 K (27 °C – 177 °C).

zero) can be obtained according to the following expression:

$$c_p = \frac{\partial Q}{\partial t} \cdot \frac{1}{\beta m} \quad (2)$$

following the three-steps procedure proposed by Coleman and co-workers (Coleman & Craig, 1996). c_p is the specific heat capacity in J g^{-1} K^{-1} and m is the mass of the sample in g. The knowledge of the specific heat capacity variation at T_g is of great importance especially in an attempt of determining the T_g of materials obtained by two (or more) miscible polymers through the Couchman–Karasz thermodynamic model (Couchman & Karasz, 1978). As can be seen from Fig. 5, the c_p at T_g associated to the baseline displacement in the 'reversing' heat flow signal for the materials made of only WG was of 0.11 J g^{-1} K^{-1}, i.e. of the same order of magnitude as the previously determined value of wheat gluten (0.22 J g^{-1} K^{-1}) (Kalichevsky, Jaroskiewicz, & Blanshard, 1992) and of the glutelin fraction of corn gluten (0.184 J g^{-1} K^{-1}) (Di Gioia, Cuq, & Guilbert, 1999). The c_p values calculated for the hybrid materials H_1 and $H_{0.5}$ were instead 0.104 J g^{-1} K^{-1} and 0.081 J g^{-1} K^{-1}, respectively, which can be ascribed to the protective (insulating) role of silica.

4.4. Microstructural observations

SEM was used to analyze the structure and morphology of both uncoated and coated samples, as shown in Fig. 6. The surface of the un-

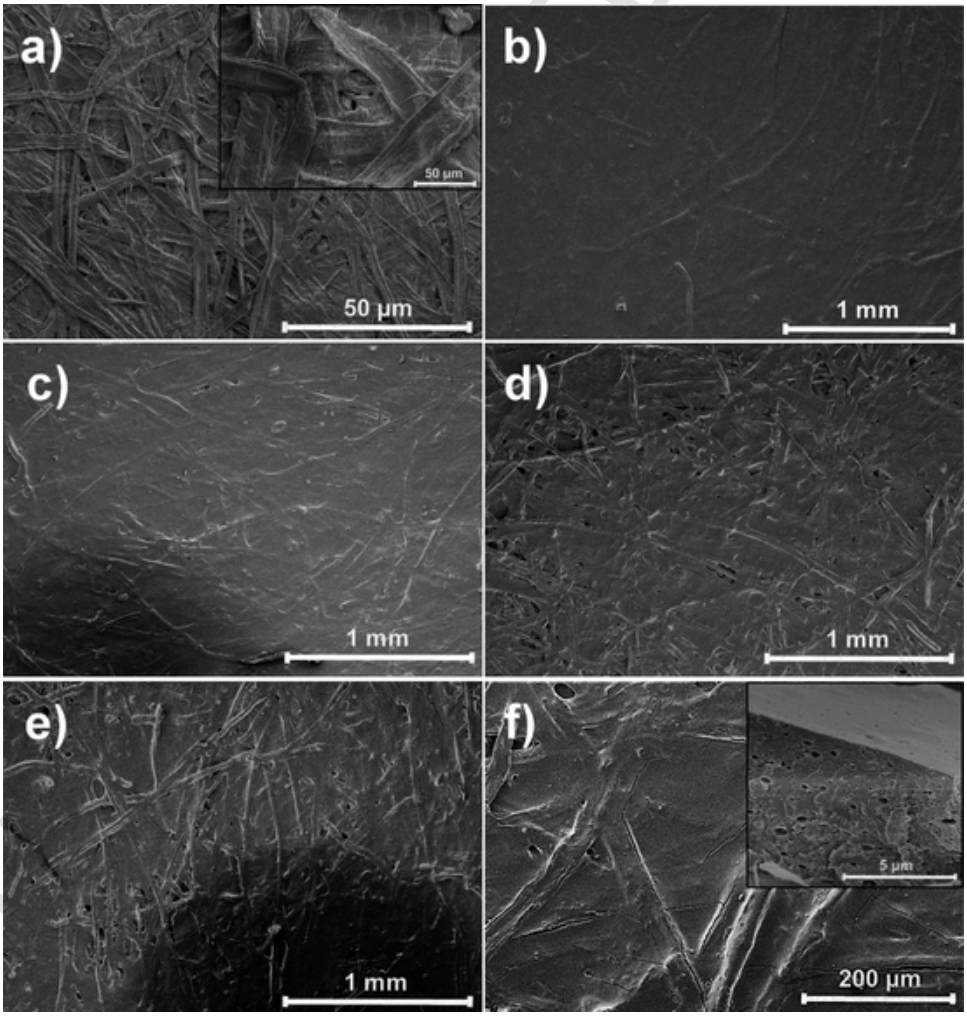

Fig. 6. SEM images of uncoated (a), WG-coated (b), and hybrid (H_3, H_1, $H_{0.5}$)-coated (c-f) paperboard samples (see the text for details).

coated paperboard shows a network of fibers of different sizes stuck, which however does not prevent the occurrence of pinholes (Fig. 6a). The deposition of the WG coating provided adequate coverage of the pristine surface. Decreasing the O/I ratio in the coating formulations (that is, moving from the formulation H_3 to the formulation $H_{0.5}$) apparently led to a less coverage of the cellulosic surface (Fig. 6c–e), which may be due to the increased ethanol (a by-product of the hydrolysis and condensation reactions of TEOS) in formulations with a higher content of the inorganic phase. It is plausible that both the increased amount of ethanol and the increasing amount of TEOS with decreasing the O/I ratio of the coating formulations, have concurrently contributed a slight penetration of the WG-based dispersion into the network of cellulosic fibers, due to changes in the rheological properties.

Noteworthy, all hybrid coatings exhibited cracks and fractures (Fig. 6f), and this trend became more obvious as the O/I ratio decreased, due to the inherent rigidity of the silica network. In agreement with previous works, these ruptures may be caused by mechanical stress, triggered by shrinking of the matrix during the solvent evaporation (Fabbri et al., 2006; Kim, 2008; Lee et al., 1999). In general, the coatings had a very smooth surface, with small crater-like dimples evenly distributed over the observed area (see the inset in Fig. 6f), which is linked to the large number of pores across the coating thickness, probably arising from air bubbles that remained trapped in the hybrid dispersion in spite of the sonication treatment performed after the coating solution preparation.

4.5. Wettability of paperboard-coated surfaces

The wettability of both neat and coated paperboard surfaces was assessed by monitoring the water droplet evolution (expressed in terms of θ, ΔV and ΔA) over 60 s, which was previously shown to be the time span where most of the total variation occurs in biopolymer coatings (Farris et al., 2011). In preliminary experiments, the contribution of evaporation phenomenon to the variation in total contact angle was quantified according to the method of Karbowiak and co-workers (Karbowiak, Debeaufort, & Voilley, 2006) by directly measuring the contact angle on a Teflon® substrate, under the assumption that neither absorption nor spreading occurs over the 60 s interval (thus, any possible variation in θ must be due to evaporation). As can be seen in Table 2 and Fig. S1, the variation in contact angle due to evaporation was approximately 2°, corresponding to droplet volume (ΔV) and surface area (ΔA) reductions of 4.5 ± 0.8 % and 3 ± 0.5 %, respectively.

The uncoated paperboard surface exhibited a fairly high initial contact angle ($\theta_0 \sim 125°$), well above 90°, which is often reported as the boundary between hydrophilic (< 90°) and hydrophobic surfaces (≥ 90°) (Lein, 2019). This can be explained by a double effect. On the one hand, according to the Wenzel's and Cassie-Bexter's theories, effects due to the presence of rough surface topography can be ruled out (Rosario et al., 2004; Wu, Zheng, & Wu, 2005). On the other hand, it is likely that the alkyl ketene dimer-based glue used in the paper manufacturing made the cellulose fibers more hydrophobic. The initial contact angle did not change significantly throughout the 60 s span, indicating that neither absorption nor spreading took place (Farris et al., 2011). In agreement with this, the evolution of both droplet volume and surface area were within the experimental evaporation range (see Fig. S2).

Deposition of pristine WG coating dramatically changed the wettability features of the paperboard substrate. Compared to the uncoated paper, θ_0 decreased to ~ 71° (see Table 2), consistent with the more hydrophilic nature of the protein biopolymer, and the fact that deposition of the WG gluten enabled nearly complete coverage of the cellulosic fibers (see Fig. 6b). After 60 s, the contact angle decreased by approximately 10° due to both spreading ($\Delta A \sim 2\%$) and absorption ($\Delta V \sim -5\%$) of the water droplet (see Fig. S2).

Addition of a small amount of silica (H_3) to the original WG-based coating formulation induced important changes in the sample, especially with respect to the water contact angle evolution. In particular, an additional decrease in θ (~ 20°) was observed as soon as the drop was placed on top of the coating (Fig. S3), because of intense spreading over the first 7 s of analysis. More specifically, the surface area of the water droplet increased by ~ 12% during this narrow time interval, but then remained rather stable for the rest of the analysis (Fig. S2). The total volume variation (ΔV) accounted for ~ -5%, indicating that absorption across the composite thickness was limited. Therefore, in line with the very high surface energy of glass and ceramics (~ 170 mJ m^{-2}), addition of a small amount of silica made the composites more wettable, while conferring resistance to water absorption during the 60 s evolution experiment.

Increasing the silica content did not result in any significant changes in θ_0 (Table 2), with a mean θ_0 value of 77° for all hybrid coatings (with the only exception of sample H_1). This unexpected behavior can be plausibly explained taking into account two opposite and counterbalancing effects: i) an increased silica content would increase the polar component of the surface free energy, thus lowering the initial contact angle; ii) increasing the silica content yielded a less coverage of the underlying cellulosic surface (as shown by the SEM analyses). Thus, it is likely that the hydrophobic properties associated with the paperboard fibers would counteract the hydrophilic properties imparted by the silica network. The same coating formulations exhibited similar final contact angle values (θ_{60}; around 67°) (Table 2) and a similar size in droplet volume variations (between -4 % and -6 %; see Fig. S2), confirming the rather moderate absorption phenomenon.

Table 2
Initial (θ_0) and final (θ_{60}) contact angle values for an uncoated Teflon® substrate, uncoated paperboard and the six biopolymer hybrid coatings.

Coating formulation	θ (°) t_0	θ (°) t_{60}
Teflon®	89.4 ± 2.9 ^{a}	87.4 ± 2.6 ^{A}
Neat paperboard	125.6 ± 7.1 ^{b}	124.3 ± 6.0 ^{B}
H_0	70.8 ± 3.8 ^{cd}	61.7 ± 2.7 ^{C} *
H_3	78.6 ± 2.8 ^{e}	53.3 ± 1.0 ^{D} *
H_2	77.7 ± 2.4 ^{e}	67.6 ± 5.8 ^{C} *
H_1	67.1 ± 4.9 ^{d}	63.1 ± 3.5 ^{C}
$H_{0.75}$	77.5 ± 5.0 ^{ce}	67.5 ± 8.4 ^{C}
$H_{0.5}$	76.1 ± 6.2 ^{ce}	67.8 ± 9.4 ^{C}

Roman superscripts denote statistically significant differences between samples (coating formulations) within the same group (t_0 and t_{60}). *Denotes statistically significant differences between groups for the same sample (the difference between θ_0 and θ_{60} for each coating formulation).

4.6. Barrier properties

Permeation of water molecules across cellulosic materials is one of the major drawbacks of these substrates, severely limiting their use in numerous applications. Biopolymer coatings can be used in reducing this permeability, thus enabling new uses for cellulosic materials without compromising the overall biodegradability of the final material. As shown in Fig. 7, a clear decrease of WVTR was observed after coating deposition (both WG and WG-silica hybrid coatings led to a WVTR reduction of ~ 37% for WG and between 63% and 74% for the hybrid coatings). Apparently, the best performance was obtained with the highest O/I ratio, that is, for the coating formulation containing the lowest amount of silica. As the amount of silica increased, the positive effect of the inorganic phase was overshadowed by the intensive cracking. The differences in WVTR between the formulations can also be explained by considering the morphology of the coatings, as displayed in Fig. 6. With increasing silica content, a less effective coverage of

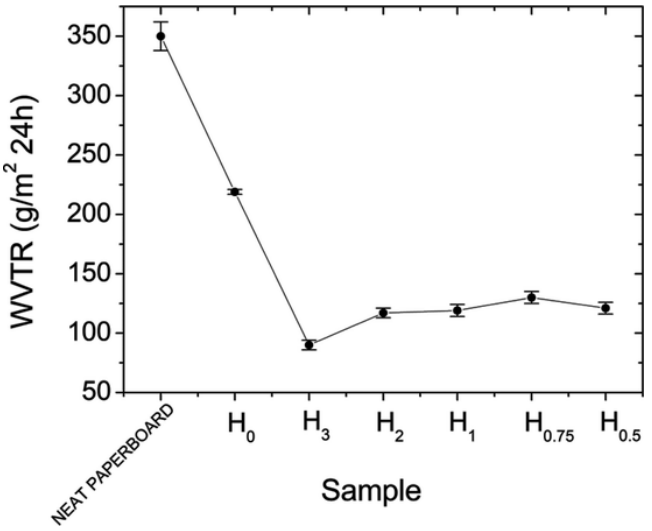

Fig. 7. Water vapor transmission rate (WVTR) measured for the neat paperboard, paperboard coated with gluten (H_0), and paperboard coated with the hybrid formulations (H_3 – $H_{0.5}$) at 23 °C and 65% RH.

the original fibrous surface was observed. Consistent with this, it is likely that the number of voids/pores and pinholes also increased, resulting in higher WVTR values. However, the result may also have been affected by differences in the intrinsic heterogeneity of the cellulosic substrate, and thus local differences in the final thickness of the whole composite (paperboard plus coating) within the same sample. Due to these considerations, in can be said that the WVTR results must be taken with care because several factors made an absolute interpretation difficult. For this reason, addressing the above issues (cracking of the coating due to internal stresses, uneven coverage of the cellulosic substrate, and penetration of coating into the fibrous network) is of utmost importance to obtain the actual barrier performance of the coatings. At the same time, if we consider that the above limitations could be addressed, the WVTR values obtained in this work are somehow encouraging, especially if compared to previous information. As reported in Table 3, our results are in line with those obtained using cellulose nanofibers (CNFs) blended with carboxy methyl cellulose (CMC) (Mazhari Mousavi et al., 2017) and polycaprolactone (PCL) (Bota et al., 2017), while being superior than those reported for zein coatings (Parris, Dickey, Wiles, Moreau, & Cooke, 2000).

However, none of the several coating solutions tested on paper/paperboard substrates led to a reduction of WVTR to values that can be deemed suitable for most food packaging applications (below ~ 5 g/m^2 24 h), confirming that a high water vapor barrier biopolymer coating for a cellulosic substrate still remains a challenge.

4.7. Safety considerations

While the functional properties of a packaging material are often regarded as the first goal to achieve, safety aspects related to food contact materials should be considered with special attention from the first steps of the design of a new packaging solution. In this study, we developed deliberately a hybrid coating by a sol-gel approach (rather than using nanoparticles, e.g., nanoclays, graphene, nanocellulose, etc.) keeping in mind that nanostructured coatings obtained by a bottom-up approach (e.g., sol-gel chemistry) do not fall into the category of nanomaterials as defined in EU Recommendation 696/2011, because they do not consist of primary particles with defined physical boundaries (Störmer, Bott, Kemmer, & Franz, 2017). It is thus reasonable to think that nanostructured materials for food contact applications can be used as long as the chemicals used to form or modify the network are authorized according to EU Regulation n. 10/2011 (Rovera et al., 2020).

5. Conclusions

In this study, we evaluated the possibility of using the sol-gel method to obtain hybrid coatings based on wheat gluten and silica to improve the water vapor resistance of wheat gluten coatings on a cellulosic substrate. In spite of the high potential of this approach to yield high-performance coatings, the experimental results highlighted some limitations of the resulting structures that hinder any possible application. In particular, the inherent rigidity of the inorganic phase led to a high degree of brittleness, to the disadvantage of the final water va-

Table 3
WVTR for paper-based materials coated with different biopolymers.

Biopolymer type	Paper type	Application	Coat wt (g/m^2)	WVTR (g/(m^2 day))	Ref.
rCNF 1%	Paperboard	Rod coater	1.6	450	Mazhari Mousavi et al., 2017
gCNF 1%	Paperboard	Rod coater	2.6	370	Mazhari Mousavi et al., 2017
rCNF 3%/CMC	Paperboard	Rod coater	6.9	400	Mazhari Mousavi et al., 2017
gCNF 3%/CMC	Paperboard	Rod coater	7.8	410	Mazhari Mousavi et al., 2017
PCL-2%	Offset printed paper board	K202 coater	N.D. (thickness ~ 6.1 μm)	533	Bota et al., 2017
PCL-2% SiO_2 + 0.5% of Al_2O_3	Offset printed paper board	K202 coater	N.D. (thickness ~ 6.1 μm)	593	Bota et al., 2017
PCL-2% SiO2 + 0.5% of ZnO	Offset printed paper board	K202 coater	N.D. (thickness ~ 6.1 μm).	512	Bota et al., 2017
CP-2	Cardboard paper	Bar coater	252.4	281	Gatto et al., 2019
CP-48	Cardboard paper	Bar coater	259.9	291	Gatto et al., 2019
Zein	Kraft paper	Spray coating	10	881	Parris et al., 2000
Chitosan-palmitic acid	Kraft paper	Wire bar coater	5.3	553	Reis, Yoshida, Reis, & Franco, 2011
Chitosan beeswax bilayer	Paper	Multicoater	3 wt%	53	Zhang et al., 2014
PLA	Paperboard	Wire bar coating	~50	9.7	Rhim et al., 2007
Starch-citric acid	Paper	Bench coater and wire wound bar	15-18	16-41	Menzel & Koch, 2014

Abbreviations: rCNF (Refiner-produced cellulose nanofiber), gCNF (grinder produced cellulose nanofiber), CMC (carboxymethyl cellulose), PCL (polycaprolactone), CP-2 (chitosan of 2% degree of acetylation), CP-2 (chitosan of 48% degree of acetylation), PLA (Poly(lactide). N.D. Not determined.

por barrier performance of the hybrid coatings. To overcome this drawback, next steps can include either the use of plasticizers or the selection of network-modifier precursors, possibly with medium-to-long aliphatic tails that would make the hybrid networks less rigid. Finally, other important functional properties (e.g., the permeability to gases, printability, sealability, and flex crack resistance) should be evaluated before market applications.

.

CRediT authorship contribution statement

Cesare Rovera: Formal analysis, Writing - review & editing. **Hasan Türe:** Methodology, Formal analysis, Writing - review & editing. **Mikael S. Hedenqvist:** Conceptualization, Methodology, Writing - review & editing, Supervision. **Stefano Farris:** Conceptualization, Methodology, Formal analysis, Writing - original draft, Writing - review & editing, Visualization, Supervision.

CRediT authorship contribution statement

Cesare Rovera: Formal analysis, Writing - review & editing. **Hasan Türe:** Methodology, Formal analysis, Writing - review & editing. **Mikael S. Hedenqvist:** Conceptualization, Methodology, Writing - review & editing, Supervision. **Stefano Farris:** Conceptualization, Methodology, Formal analysis, Writing - original draft, Writing - review & editing, Visualization, Supervision.

Appendix A. Supplementary data

Supplementary material related to this article can be found, in the online version, at doi:https://doi.org/10.1016/j.fpsl.2020.100561.

References

Andersson, C (2009). New ways to enhance the functionality of paperboard by surface treatment – a review. Packaging Technology and Science, 21, 339–373. doi:10.1002/pts.823.

Bandyopadhyay, A, De Sarkar, M, & Bhowmick, A (2005). Poly(vinyl alcohol)/silica hybrid nanocomposites by sol-gel technique: synthesis and properties. Journal of Materials Science, 40, 5233–5241. doi:10.1007/s10853-005-4417-y.

Bossi, E, Tana, F, Punta, C, Cigada, A, & De Nardo, L (2016). Flexible hybrid coatings with efficient antioxidation properties. Food Packaging and Shelf Life, 10, 106–114. doi:10.1016/j.fpsl.2016.10.002.

Bota, J, Kratofil, K L, Katančić, Z, Brozović, M, & Hrnjak-Murgić, Z (2017). Surface characteristics and enhancement of water vapour properties of paperboard coated with polycaprolactone nanocomposites. Journal of Adhesion Science and Technology, 31, 466–486. doi:10.1080/01694243.2016.1218313.

Cho, S W, Gällstedt, M, & Hedenqvist, M S (2010). Properties of wheat gluten/poly(lactic acid) laminates. Journal of Agricultural and Food Chemistry, 58, 7344–7350. doi:10.1021/jf1003144.

Cho, S W, Gällstedt, M, Johansson, E, & Hedenqvist, M S (2011). Injection-molded nanocomposites and materials based on wheat gluten. International Journal of Biological Macromolecules, 48, 146–152. doi:10.1016/j.ijbiomac.2010.10.012.

Coleman, N J, & Craig, Q M D (1996). Modulated temperature differential scanning calorimetry: a novel approach to pharmaceutical thermal analysis. International Journal of Pharmaceutics, 135, 13–29. doi:10.1016/0378-5173(95)04463-9.

Corradini, C, Alfieri, I, Cavazza, A, Lantano, C, Lorenzi, A, & Zucchetto, N, et al. (2013). Antimicrobial films containing lysozyme for active packaging obtained by sol–gel technique. Journal of Food Engineering, 119, 580–587. doi:10.1016/j.jfoodeng.2013.05.046.

Couchman, P R, & Karasz, F E (1978). A classical thermodynamic discussion of the effect of composition on glass-transition temperatures. Macromolecules, 11, 117–119. doi:10.1021/ma60061a021.

Das, O, Loho, T A, Capezza, A J, Lemrhari, I, & Hedenqvist, M S (2018). A novel way of adhering PET onto protein (Wheat Gluten) plastics to impart water resistance. Coatings, 8, 388. doi:10.3390/COATINGS8110388.

Das, O, Capezza, A J, Mårtensson, J, Dong, Y, Neisiany, R E, & Pelcastre, L, et al. (2020). The effect of carbon black on the properties of plasticised wheat gluten biopolymer. Molecules, 25, 2279. doi:10.3390/molecules25102279.

Deshwal, G K, Panjagari, N R, & Alam, T (2019). An overview of paper and paper based food packaging materials: health safety and environmental concerns. Journal of Food Science and Technology, 56, 4391–4403. doi:10.1007/s13197-019-03950-z.

Di Gioia, L, Cuq, B, & Guilbert, S (1999). Thermal properties of corn gluten meal and its proteic components. International Journal of Biological Macromolecules, 24, 341–350. doi:10.1016/S0141-8130(99)00048-3.

Fabbri, P, Singh, B, Leterrier, Y, Manson, J A E, Messori, M, & Pilati, F (2006). Cohesive and adhesive properties of polycaprolactone/silica hybrid coatings on poly(methyl methacrylate) substrates. Surface and Coatings Technology, 200, 6706–6712. doi:10.1016/j.surfcoat.2005.10.003.

Farrell, A E, Plevin, R J, Turner, B T, Jones, A D, O'Hare, M, & Kammen, D M (2006). Ethanol can contribute to energy and environmental goals. Science, 311, 506–508. doi:10.1126/science.1121416.

Farris, S, Introzzi, L, Biagioni, P, Holz, T, Schiraldi, A, & Piergiovanni, L (2011). Wetting of biopolymer coatings: contact angle kinetics and image analysis investigation. Langmuir, 27, 7563–7574. doi:10.1021/la2017006.

Farris, S, Introzzi, L, Fuentes-Alventosa, J M, Santo, N, Rocca, R, & Piergiovanni, L (2012). Self-assembled pullulan-silica oxygen barrier hybrid coatings for food packaging applications. Journal of Agricultural and Food Chemistry, 60, 782–790. doi:10.1021/jf204033d.

Fuentes-Alventosa, J M, Introzzi, L, Santo, N, Cerri, G, Brundu, A, & Farris, S (2013). Self-assembled nanostructured biohybrid coatings by an integrated "sol-gel – intercalation" approach. RSC Advances, 3, 25086–25096. doi:10.1039/C3RA45640D.

Gällstedt, M, Brottman, A, & Hedenqvist, M S (2005). Packaging-related properties of protein- and chitosan-coated paper. Packaging Technology and Science, 18, 16–170. doi:10.1002/pts.685.

Gatto, M, Ochi, D, Pedroso Yoshida, C M, & Ferreira da Silva, C (2019). Study of chitosan with different degrees of acetylation as cardboard paper coating. Carbohydrate Polymers, 210, 56–63. doi:10.1016/j.carbpol.2019.01.053.

Gennadios, A, Brandenburg, A H, Park, J W, Weller, C L, & Testin, R F (1994). Water vapor permeability of wheat gluten and soy protein isolate films. Industrial Crops and Products, 2, 189–195. doi:10.1016/0926-6690(94)90035-3.

Gontard, N, Guilbert, S, & Cuq, J L (1992). Edible wheat gluten films: Influence of the main process variables on film properties using response-surface methodology. Journal of Food Science, 57, 190–195. doi:10.1111/j.1365-2621.1992.tb05453.x.

Gontard, N, Thibault, R, Cuq, B, & Guilbert, S (1996). Influence of relative humidity and film composition on oxygen and carbon dioxide permeabilities of edible films. Journal of Agricultural and Food Chemistry, 44, 1064–1069. doi:10.1021/jf9504327.

Guillaume, C, Pinte, J, Gontard, N, & Gastaldi, E (2010). Wheat gluten-coated papers for bio-based food packaging: structure, surface and transfer properties. Food Research International, 43, 1395–1401. doi:10.1016/j.foodres.2010.04.014.

Hatakeyama, T, & Quinn, F X (1999). Thermal Analysis: Fundamentals and Applications to Polymer Science (2nd ed.). New York: John Wiley and Sons.

Hedenqvist, M S (2018). Barrier packaging materials. In Kutz, M (Ed.), Handbook of Environmental Degradation of Materials (pp. 559–581). Amsterdam: Elsevier, Inc..

Jones, P, & Comfort, D (2017). The forest, paper and packaging industry and sustainability. International Journal of Sales, Retailing and Marketing, 6, 3–21.

Kalichevsky, M T, Jaroskiewicz, E M, & Blanshard, J M V (1992). Glass transition of gluten. 1: Gluten and gluten-sugar mixtures. International Journal of Biological Macromolecules, 14, 257–266. doi:10.1016/S0141-8130(05)80038-8.

Karbowiak, T, Debeaufort, F, & Voilley, A (2006). Importance of surface tension characterization for food, pharmaceutical and packaging products: a review. Critical Reviews in Food Science and Nutrition, 46, 391–407. doi:10.1080/10408390591000884.

Kim, S W (2008). Preparation and barrier property of poly(vinyl alcohol)/SiO2 hybrid coating films. Korean Journal of Chemical Engineering, 25, 1195–1200. doi:10.1007/s11814-008-0197-9.

Krimm, S, & Bandekar, J (1986). Vibrational spectroscopy and conformation of peptides, polypeptides, and proteins. Advances in Protein Chemistry, 38, 181–364. doi:10.1016/S0065-3233(08)60528-8.

Krook, M, & Hedenqvist, M S (2002). Polymer–clay nanocomposites, one way to improve the barrier properties of polymers used in packaging. Conference proceedings from the Tappi place conf.

Lantano, C, Alfieri, I, Cavazza, A, Corradini, C, Lorenzi, A, & Zucchetto, N, et al. (2014). Natamycin based sol–gel antimicrobial coatings on polylactic acid films for food packaging. Food Chemistry, 165, 342–347. doi:10.1016/j.foodchem.2014.05.066.

Lee, S Y, Lee, J D, & Yang, S M (1999). Preparation of silica-based hybrid materials coated on polypropylene film. Journal of Materials Science, 34, 1233–1241. doi:10.1023/A:1004517208507.

Lein, H L (2019). Coatings and surfaces with hydrophobic and anti-icing properties. In Benelmekki, M, & Erbe, A (Eds.), Nanostructured Thin Films (pp. 257–269). Amsterdam: Elsevier, Inc.

Lens, J P, de Graaf, L A, Stevels, W M, Dietz, C H J T, Verhelst, K C S, & Vereijken, J M, et al. (2003). Influence of processing and storage conditions on the mechanical and barrier properties of films cast from aqueous wheat gluten dispersions. Industrial Crops and Products, 17, 119–130. doi:10.1016/S0926-6690(02)00092-4.

Liu, X, Chen, K, Wang, J, Wang, Y, Tang, Y, & Gao, X, et al. (2020). An on-package colorimetric sensing label based on a sol-gel matrix for fish freshness monitoring. Food Chemistry, 307, 125580. doi:10.1016/j.foodchem.2019.125580.

Mascheroni, E, Guillard, V, Gastaldi, E, Gontard, N, & Chalier, P (2011). Anti-microbial effectiveness of relative humidity-controlled carvacrol release from wheat gluten/montmorillonite coated papers. Food Control, 22, 1582–1591. doi:10.1016/j.foodcont.2011.03.014.

Mazhari Mousavi, S M, Afra, E, Tajvidi, M, Bousfiled, D W, & Dehghani-Firouzabadi, M (2017). Cellulose nanofiber/carboxymethyl cellulose blends as an efficient coating to improve the structure and barrier properties of paperboard. Cellulose, 24, 3001–3014. doi:10.1007/s10570-017-1299-5.

Menzel, C, & Koch, K (2014). Impact of the coating process on the molecular structure of starch-based barrier coatings. Journal of Applied Polymer Science, 131, 1–9. doi:10.1002/app.41190.

Minelli, M, De Angelis, M G, Doghieri, F, Rocchetti, M, & Montenero, A (2010). Barrier properties of organic-inorganic hybrid coatings based on polyvinyl alcohol with improved water resistance. Polymer Engineering & Science, 50, 144–153. doi:10.1002/pen.21440.

Mir, S A, Wani, H M, Wani, I A, Singh, P, & Wani, A A (2017). Testing of paper as packaging material for food industry. In Singh, P, Wani, A A, & Langowski, H C (Eds.), Food packaging materials-testing and quality assurance. Boca Raton: CRC Press. (ch. 8).

Mirmehdi, S, Gherardi Hein, P R, Grígoli de Luca Sarantópoulos, C I, Dias, M V, & Denzin Tonoli, G H (2018). Cellulose nanofibrils/nanoclay hybrid composite as a paper coating: Effect of spray time, nanoclay content and corona discharge on barrier and mechanical properties of the coated papers. Food Packaging and Shelf Life, 15, 87–94. doi:10.1016/j.fpsl.2017.11.007.

Mujica Paz, H, & Gontard, N (1997). Oxygen and carbon dioxide permeability of wheat gluten film: Effect of relative humidity and temperature. Journal of Agricultural and Food Chemistry, 45, 4101–4105. doi:10.1021/jf970201v.

Mujica Paz, H, Guillard, V, Reynes, M, & Gontard, N (2005). Ethylene permeability of wheat gluten film as a function of temperature and relative humidity. Journal of Membrane Science, 256, 108–115. doi:10.1016/j.memsci.2005.02.011.

Olabarrieta, I, Cho, S W, Gällstedt, M, Sarasua, J R, Johansson, E, & Hedenqvist, M (2006). Aging prperties of films of plasticized vital wheat gluten cast from acidic and basic solutions. Biomacromolecules, 7, 1657–1664. doi:10.1021/bm0600973.

Ottesen, V, Kumar, V, Toivakka, M, Chinga-Carrasco, G, Syverud, K, & Gregersen, ØW (2017). Viability and properties of roll-to-roll coating of cellulose nanofibrils on recycled paperboard. Nordic Pulp & Paper Research Journal, 32, 179–188. doi:10.3183/npprj-2017-32-02-p179-188.

Parris, N, Dickey, L C, Wiles, J L, Moreau, R A, & Cooke, P H (2000). Enzymatic hydrolysis, grease permeation and water barrier properties of zein isolate coated paper. Journal of Agricultural and Food Chemistry, 48, 890–894. doi:10.1021/jf991079y.

Razavi, R, Tajik, H, Moradi, M, Molaei, R, & Ezati, P (2020). Antimicrobial, microscopic and spectroscopic properties of cellulose paper coated with chitosan sol-gel solution formulated by epsilon-poly-l-lysine and its application in active food packaging. Carbohydrate Research, 489, 107912. doi:10.1016/j.carres.2020.107912.

Reis, A B, Yoshida, C M P, Reis, Ana Paula C, & Franco, T T (2011). Application of chitosan emulsion as a coating on Kraft paper. Polymer International, 60, 963–969. doi:10.1002/pi.3023.

Rhim, J W, Lee, J-H, & Hong, S-I (2007). Increase in water resistance of paperboard by coating with poly(lactide). Packaging Technology and Science, 20, 393–402. doi:10.1002/pts.767.

Rosario, R, Gust, D, Garcia, A A, Hayes, M, Taraci, J L, & Clement, T, et al. (2004). Lotus effect amplifies light-induced contact angle switching. The Journal of Physical Chemistry B, 108, 12640–12642. doi:10.1021/jp0473568.

Rovera, C, Ghaani, M, & Farris, S (2020). Nano-inspired oxygen barrier coatings for food packaging applications: an overview. Trends in Food Science & Technology, 97, 210–220. doi:10.1016/j.tifs.2020.01.024.

Sartori, T, Feltre, G, do Amaral Sobral, P J, Lopes da Cunha, R, & Mengalli, F C (2018). Properties of films produced from blends of pectin and gluten. Food Packaging and Shelf Life, 18, 221–229. doi:10.1016/j.fpsl.2018.11.007.

Schubert, U (2015). Chemistry and Fundamentals of the Sol-Gel Process. In Levy, D, & Zayat, M (Eds.), The Sol-Gel Handbook (pp. 3–27). Weinheim: Wiley-VCH Verlag GmbH & Co. KGaA.

Startek, K, Marczak, J, & Lukowiak, A (2020). Oxygen barrier enhancement of polymeric foil by sol-gel-derived hybrid silica layers. Polymers, 195, 122437. doi:10.1016/j.polymer.2020.122437.

Störmer, A, Bott, J, Kemmer, D, & Franz, R (2017). Critical review of the migration potential of nanoparticles in food contact plastics. Trends in Food Science & Technology, 63, 39–50. doi:10.1016/j.tifs.2017.01.011.

Tong, Q, Xiao, Q, & Lim, L T (2008). Preparation and properties of pullulan–alginate–carboxymethylcellulose blend films. Food Research International, 41, 1007–1014. doi:10.1016/j.foodres.2008.08.005.

Tunc, S, Angellier, H, Cahyana, Y, Chalier, P, Gontard, N, & Gastaldi, E (2007). Functional properties of wheat gluten/montmorillonite nanocomposite films processed by casting. Journal of Membrane Science, 289, 159–168. doi:10.1016/j.memsci.2006.11.050.

Türe, H, Blomfeldt, T O J, Gällstedt, M, Hedenqvist, M S, & Farris, S (2013). Nanostructured silica/wheat gluten hybrid materials prepared by catalytic sol-gel chemistry. Macromolecular Chemistry and Physics, 214, 1131–1139. doi:10.1002/macp.201200646.

Türe, H, Gällstedt, M, Johansson, E, & Hedenqvist, M S (2013). Wheat-gluten/montmorillonite clay multilayer-coated paperboards with high barrier properties. Industrial Crops and Produtcs, 51, 1–6. doi:10.1016/j.indcrop.2013.08.054.

Uragami, T, Okazaki, K, Matsugi, H, & Miyata, T (2002). Structure and permeation characteristics of an aqueous ethanol solution of organic-inorganic hybrid membranes composed of poly(vinyl alcohol) and tetraethoxysilane. Macromolecules, 35, 9156–9163. doi:10.1021/ma020850u.

Wu, X, Zheng, L, & Wu, D (2005). Fabrication of superhydrophobic surfaces from microstructured ZnO-based surfaces via a wet-chemical route. Langmuir, 21, 2665–2667. doi:10.1021/la050275y.

Wu, Q, Andersson, R L, Holgate, T, Johansson, E, Gedde, U W, & Olsson, R T, et al. (2014). Highly porous flame-retardant and sustainable biofoams based on wheat gluten and in situ polymerized silica. Journal of Materials Chemistry A, 2, 20996–21009. doi:10.1039/c4ta04787g.

Zhang, W, Xiao, H, & Qian, L (2014). Enhanced water vapour barrier and grease resistance of paper bilayer-coated with chitosan and beeswax. Carbohydrate Polymers, 101, 401–406. doi:10.1016/j.carbpol.2013.09.097.